



Hydroxypropyl sulfonated starch and *Aspergillus oryzae* biomass for cationic dye adsorption: characterization, mechanism, sorption modelling

A. Hashem¹ · Chukwunonso O. Aniagor² · L. A. Mohamed³ · Abdelrahman M. Abdelgawad¹ · A. A. Aly¹

Received: 14 September 2023 / Revised: 5 December 2023 / Accepted: 15 December 2023
© The Author(s) 2024

Abstract

In this work, hydroxypropyl starch sulfate (HPSS) and *Aspergillus oryzae* (*Asp. oryzae*) were successfully synthesized and investigated for aqueous methylene blue (MB) adsorption. The as-prepared adsorbents were also characterized extensively using FTIR, XRD, SEM, EDX, and BET surface area analyses to elucidate their functional, textural, and morphological properties. Also, the effects of initial dye concentration, contact time, and pH on the adsorption performance of both adsorbents were systematically investigated. Due to the significant surface area differences, the HPSS recorded a higher maximum adsorption capacity (q_{\max}) of 52.41 mg/g at 20 mg/L initial concentration, 60 min, and pH 8.0, while the *Asp. oryzae* recorded a q_{\max} of 37.26 mg/g at 20 mg/L initial concentration, 60 min, and pH 9.0. Specifically, the $-\text{SO}_3$ groups on the HPSS shared some electrostatic affinity with the MB dye cationic center (N^+ backbone), while a hydrogen bond is formed between the hydroxyl groups of the starch and N^+ backbone of the MB dye. Also, the nitrogen- and oxygen-containing groups on the *Asp. oryzae* provided active sites for the binding of MB species. Also, the XRD spectra of the loaded HPSS showed a decrease in the sharp crystalline peaks, while no structural changes were observed in the case of loaded *Asp. oryzae*. Therefore, the effectiveness of the HPSS and *Asp. oryzae* for adsorbing MB was established in the study.

Keywords Dye removal · Methylene blue · Sulfonated starch · Adsorption modelling · Fungal-based adsorbent

1 Introduction

Methylene blue (MB) is a cationic dye with extensive industrial applications [1]. Despite its seemingly mild toxicity, ingestion of MB-contaminated water, like in the case of every other organic pollutant, could be detrimental to human and animal health—cases of increased heart rate, diarrhea, dizziness, and vomiting as a result of ingesting water with a mild (< 100 mg/L) concentration of MB abound. Similarly,

painful micturition, severe headache, and methemoglobinemia could be experienced following accidental ingestion of a large MB concentration (> 150 mg/L) [2]. Due to the concerns for environmental safety and sustainability, the removal of dyes and pigments from waste has been a front-burner issue over the last decade. Consequently, different techniques exist for the efficient treatment of dye-contaminated streams such as degradation [3–5], flocculation–coagulation [6, 7], oxidation [8, 9], membrane filtration [10], ion exchange resins [11], and adsorption [12, 13]. Due to its applicational flexibility, cost-effectiveness, and process efficiency, the adsorption technique has been preferred. Meanwhile, different natural, synthetic, and hybrid adsorbents have been applied to methylene blue adsorption.

Notably, starch-based adsorbents are cheap, renewable, and environmentally friendly. Also, the reactive hydroxyl groups present in the starch molecules improve their chemical stability and reactivity. The hydroxyl groups also make starch molecules readily tunable into the array of useful derivatives and biopolymers. Chen et al. [14] prepared starch-humic acid composite hydrogel beads which were

✉ A. Hashem
alihazem2000@yahoo.com

✉ Chukwunonso O. Aniagor
co.aniagor@unizik.edu.ng

¹ Textile Research and Technology Institute, National Research Centre, Dokki, Cairo, Egypt

² Department of Chemical Engineering, Nnamdi Azikiwe University, P.M.B. 5025, Awka, Nigeria

³ Biotechnology Research Institute, National Research Centre, Dokki, Cairo, Egypt

applied for MB adsorption. The study reported preferential adsorption of MB molecules at an acidic pH range with a predominant π - π interaction and ion exchange. Similarly, the starch-based high-performance hydrogel was fabricated by Chen et al. [15] by crosslinking polyacrylic acid-g-starch with N, N'-methylene-bisacrylamide. The as-prepared adsorbent was used for the adsorption of aqueous MB. It was noted that the carboxylic and hydroxy groups on the hybrid adsorbent enhanced MB adsorption via hydrogen bonding and electrostatic interaction mechanism. Furthermore, starch/rice husk ash-based superabsorbent composite [16], bioinspired catecholamine/starch superabsorbent [17], biodegradable superabsorbent cassava starch-based hydrogel [18], and succinylated starch nanocrystals [19] were all prepared and effectively utilized for MB adsorption.

Additionally, numerous studies have explored and successfully reported on the use of other agro materials, including microbial biomass, as viable low-cost alternative adsorbents for dye wastewater treatment. Congo red dye was successfully adsorbed onto *Trametes versicolor* biomass by Munagapati et al. [20], and a maximum adsorption capacity of 415.7 mg/g was obtained at pH 2.0 and 60 °C. Furthermore, reasonable process efficiencies were reported during the respective adsorption of aqueous reactive red 3 and reactive green 6 dye onto *Trichoderma harzianum* ($q_{\text{max}} = 172.63$) [21] and immobilized *Aspergillus* sp. ($q_{\text{max}} = 21.2$ mg/g) [22] biomasses.

Thus, using methylene blue (MB) dye as the model pollutant, this work investigates the adsorptive potentials of sulfonated starch (HPSS) and *Aspergillus oryzae* (*Asp. oryzae*) biomass. The following benefits can be obtained by using microbial biomass as an adsorbent: (i) they can be quickly and easily cultivated on low-cost medium using simple methods, (ii) they exhibit exceptional surface complexation capabilities because of the many functional groups that make up their cell walls, and (iii) they are often non-pathogenic and so safe for use in water treatment. Because of their greater surface area, stronger mechanical strength,

cost-effectiveness, and applicational flexibility, dead fungal biomass was specifically chosen in this study [23]. Although Hebeish and Aly [24] previously studied the adsorption of MB using starch hydroxypropyl sulfate, the instrumental characterization of the prepared adsorbent was not extensively conducted and discussed. Similarly, the adsorption studies were limited only to the effect of process variables (pH, initial dye concentration, time, and adsorbent dose). This present study extensively characterized the prepared starch sulfate including the structural, textural, morphological, elemental distribution, and pore distribution analyses. This study also compared the adsorptive performance of the HPSS to that of *Asp. oryzae* via an in-depth discussion on the isotherm and kinetics modelling, as well as the plausible adsorption mechanisms.

2 Material and methods

2.1 Materials

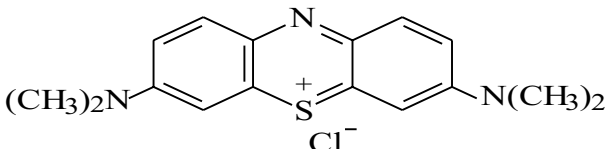
The Cairo Company for Starch and Glucose supplied the maize starch used in the study, and the culture collection center at the Department of Microbial Chemistry, National Research Center, Cairo, Egypt, graciously provided the *Asp. oryzae* strain. All other reagents, methylene blue, sodium bisulphite, hydrochloric acid, sodium hydroxide, epichlorohydrin, and ethanol, were laboratory-grade chemicals (Merck, Germany). The molecular formula, molecular weight, maximum wavelength, and structure of the dye are listed in Table 1.

2.2 Methods

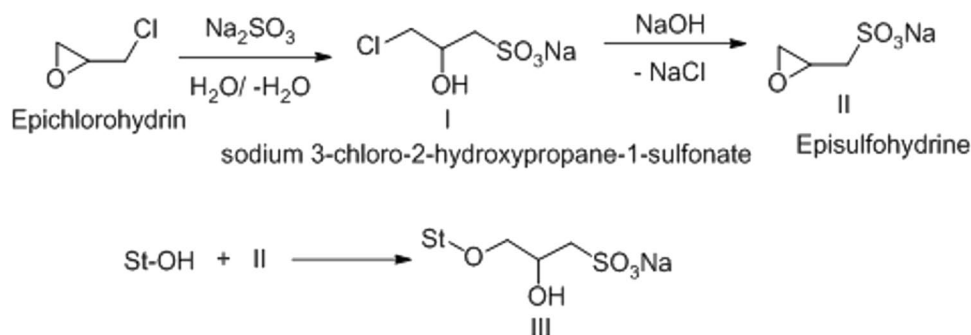
2.2.1 Preparation of the *Asp. oryzae* biomass

The culture substrate employed in this study was potato dextrose broth (PDB), and our earlier publications [25]

Table 1 General characteristics of methylene blue (MB)

Properties	
Molecular formula:	$\text{C}_{16}\text{H}_{18}\text{ClN}_3\text{S}$
Molecular weight:	319.8
Maximum wavelength	663 nm
Structure:	

Scheme 1 Preparation of hydroxypropyl hydroxypropyl sulfonated starch (HPSS)



have a detailed technique for the fungus cultivation, as well as the mycelium development, and extraction. After a successful extraction, the fungal mycelium was thoroughly washed, oven-dried at 50 °C until it reached a constant dry weight, and then ground to a fine particle size (~50–125 μm).

2.2.2 Preparation of 2-hydroxy-3-chloropropyl sulfate

In the procedure, 1,2-propanediol (1.7 mL, 20 mmol) was introduced into sodium sulfite solution (2.52 g, 20 mmol) contained in a 250-mL conical flask. The resultant emulsion was stirred at 25 °C for 72 h until a clear solution was achieved. Subsequent freeze-drying of the clear solution afforded a gelatinous solid which metamorphosed to a powdery suspension after an overnight stirring with the addition of ethanol (40 mL). The suspension was boiled, filtered while hot (using a sintered glass), and washed with boiling ethanol (25 mL). Upon cooling, the resultant crystals were obtained as filtrate, washed with ethanol, and oven-dried to give a water-soluble whitish monohydrated product. Notably, the NaOH produced during the epoxide ring opening converts some HSO_3^- to SO_3^{2-} , thus facilitating the attack of SO_3^{2-} on $-\text{CH}_2-\text{Cl}$ and producing episulfohydrin.

2.2.3 Synthesis of hydroxypropyl starch sulfate

Sodium hydroxide (NaOH) powder was mixed with neat starch in a dry state using a mechanical stirrer. Then, 2-hydroxy-3-chloropropyl sulfate (in a molar ratio of 1: 1.5 with the NaOH powder) was added to the blended mixture of starch/sodium hydroxide at room temperature. The reactant was transferred to a stoppered bottle, with its temperature maintained at 90 °C for 60 min using a thermostated water bath. The reaction was terminated by pouring 200 mL ethanol with a pH adjustment to pH 8.0. The product was filtered off and then purified with 80% v/v of ethanol in a Soxhlet apparatus for 12 h. This is considered a final step which was followed by a subsequent drying of the product (Scheme 1).

2.2.4 Batch adsorption studies

The detailed protocol for the equilibrium and kinetic experiments has been reported previously by the authors. The experiment was conducted at the following reaction conditions: HPSS dosage, 0.2 g/L; initial dye concentration, 10–100 mg/L; temperature, 30 °C; stirring speed, 200 rpm; contact time, 0–180 min. The amount of MB adsorbed at each instant (q_t , mg/g) and equilibrium (q_e , mg/g) is evaluated from Eqs. (1) and (2), respectively.

$$q_t = \frac{(C_o - C_t) \times V}{W} \quad (1)$$

$$q_e = \frac{(C_o - C_e) \times V}{W} \quad (2)$$

where C_o (mg/L), C_e (mg/L), and C_t (mg/L) are the initial, equilibrium, and instantaneous dye concentrations, respectively. V (L) is the volume of adsorbate solution used, and W (g) is the mass of the adsorbent.

2.3 Adsorption isotherm and kinetic modelling

For the isotherm studies, the following 2-parameter [Langmuir, Eq. (3); Freundlich, Eq. (4), and Temkin, Eq. (5)] and 3-parameter [Redlich-Peterson, Eq. (6); Hills, Eq. (7); Sip, Eq. (8); Toth, Eq. (9) and Khan, Eq. (10)] nonlinear models were investigated. The Langmuir and Freundlich models are employed to respectively describe homogeneous and heterogeneous adsorption systems [26]. The Temkin equation applies to studying the adsorption energy in a dominant chemisorption process [27]. The Redlich-Peterson, Hill, Sips, Toth, and Khan models are 3-parameter isotherms that are based on Langmuir and Freundlich model characteristics. Specifically, the Redlich-Peterson model follows a hybrid mix of the monolayer and multi-layer adsorption sorption mechanisms [28]. The Hills model explains solute binding onto homogeneous substrates as a cooperative monolayer binding onto non-uniform sites of the same adsorbent.

The cooperative phenomenon implies that solute binding on one site could influence the energy and stability of the other binding sites on the same adsorbent. The Sip model is an upgraded form of the Freundlich model, with features for circumventing the Freundlich model limitations at high adsorbate concentrations [27]. The Toth model postulates a variable energy distribution where the energies of the minimum adsorption site energies fell short of the peak energy values [29].

$$q_e = \frac{q_{\max} K_L C_e}{1 + K_L C_e} \quad (3)$$

$$q_e = K_F C_e^{1/n} \quad (4)$$

$$q_e = \frac{RT}{b_T} \ln(A_T C_e) \quad (5)$$

$$q_e = \frac{K_{RP} C_e}{1 + \alpha_{RP} (C_e)^g} \quad (6)$$

$$q_e = \frac{q_{mH} C_e^{n_H}}{K_H + C_e^{n_H}} \quad (7)$$

$$q_e = \frac{K_s \times C_e^\beta}{1 + a_s * C_e^\beta} \quad (8)$$

$$q_e = \frac{k_T \times C_e}{(a_T + C_e)^{r-1}} \quad (9)$$

$$q_e = \frac{q_{mK} b_K C_e}{(1 + b_K C_e)^{a_K}} \quad (10)$$

[a_K , Kahn isotherm model exponent; b_K , Khan isotherm model constant; q_m , maximum adsorption capacity (mg/g); K_s , Sips isotherm model constant (L/g); β , Sips isotherm exponent; a_s , Sips isotherm model constant (L/g); a_R , Redlich-Peterson isotherm constant (1/mg); a_T , Toth isotherm constant (L/mg); g , Redlich-Peterson exponent that lies between 0 and 1; K_R , Redlich-Peterson isotherm constant (L/g); K_S , Sips isotherm model constant (L/g); n_H , Hill cooperativity coefficient of the binding interaction; q_{SH} , Hill isotherm maximum uptake saturation (mg/L); K_L , Langmuir adsorption constant (L/mg); K_F , Freundlich constant; K_D , Hill isotherm constant].

For the kinetic studies, the following nonlinear 2-parameter [pseudo-first-order, Eq. (11), pseudo-second-order, Eq. (12), Elovich, Eq. (13), and the linear form of the Intraparticle diffusion, Eq. (14)] models were investigated. The

pseudo-first-order (PFO) model assumes an effective proportionality between the rate of sorption site occupation and the number of unoccupied sites [30, 31], while for the pseudo-second-order (PSO) model, the extent of adsorption is a function of the solute accessibility to the adsorbent sorption site [31]. The second-order kinetic description of an adsorption system containing adsorbents with an energetically heterogeneous surface is achieved using the Elovich model. The intraparticle diffusion postulates a proportional variation between the solute uptake and the square root of adsorption time [32].

$$q_t = q_e [1 - \exp(-K_1 t)] \quad (11)$$

$$q_t = \frac{K_2 \times q_e^2 \times t}{1 + K_2 \times q_e \times t} \quad (12)$$

$$q_t = \left(\frac{1}{\beta}\right) \ln(1 + \alpha \beta t) \quad (13)$$

$$q_t = K_{id} \sqrt{t} + C \quad (14)$$

[k_1 , pseudo-first-order rate constant (1/min); k_2 , pseudo-second-order rate constant (g/mg × min); α , Elovich's initial adsorption rate (mg/g × min), β , Elovich's desorption constant (g/mg); k_{id} , intraparticle diffusion rate constant; K_b , Bangham model constants; n , Bangham model exponent].

Table 2 Mathematical expression of the error models

Error function	Equation	Eq. no
ARE	$\sum_{i=1}^n \left \frac{q_{e,exp} - q_{e,cal}}{q_{e,exp}} \right $	(15)
APE	$\frac{\sum_{i=1}^n (q_{e,exp} - q_{e,cal})/q_{e,exp} }{N} \times 100$	(16)
ERRSQ	$\sum_{i=1}^n [q_{e,cal} - q_{e,exp}]^2$	(17)
Hybrid	$\frac{100}{n-p} \sum_{i=1}^n \left[\frac{(q_{e,exp} - q_{e,cal})^2}{q_{e,exp}} \right]$	(18)
MPSD	$100 \times \sqrt{\frac{1}{n-p} \sum_{i=1}^n \left[\frac{(q_{e,exp} - q_{e,cal})}{q_{e,exp}} \right]^2}$	(19)
χ^2	$\sum \frac{(q_{e,exp} - q_{e,cal})^2}{q_{e,exp}}$	(20)
R^2	$\frac{\sum (q_{e,cal} - q_{e,exp})^2}{\sum (q_{e,cal} - q_{e,exp})^2 + \sum (q_{e,exp} - q_{e,cal})^2}$	(21)

n number of data points, p number of the model parameter

2.4 Error analysis

The fitting goodness of nonlinear models is generally determined using specialized error models. Table 2 presents the mathematical expression of the different error models adopted in the study. Meanwhile, by applying different error models, varying error values were also generated. Hence, to ensure a holistic model analysis, these error values were normalized following the procedure we previously reported [33] to generate the sum of normalized error (SNE) values.

3 Results and discussion

3.1 Characterization of HPSS

3.1.1 Surface chemistry

Fourier transform spectroscopy (FTIR) spectra of the HPSS and *Asp. oryzae* samples were determined using a PerkinElmer spectrophotometer within the 4000 to 400 cm^{-1} range. The generated FTIR spectra are shown in Fig. 1a, b. For the FTIR spectrum of native starch (black line in Fig. 1a), the glucose unit of the starch gave rise to the -OH and C-O stretching vibration band at 3321 cm^{-1} and 994 cm^{-1} , respectively. The -OH in-plane bending vibration of the glucose unit and the -CH_2 groups are respectively attributed to the bands at 1328 and 2924 cm^{-1} . Comparison of the FTIR spectrum of HPSS (red line in Fig. 1a) with that of the native starch respectively shows the appearance of -SO_3 asymmetric and symmetric stretching vibration at 1459 and 1221 cm^{-1} , while the C-O-S stretching vibration is registered at 816 cm^{-1} . Additionally, the sulfate groups can be observed at around 701 and 612 cm^{-1} . The aforementioned sulfate groups are indications of the successful preparation of the HPSS sample. The MB@HPSS spectrum (green line in Fig. 1a) exhibits a slight shift in the

wavenumber peaks which are responsible for MB adsorption. For instance, the -NH/-OH overlapped stretching vibration shifted from 3321 cm^{-1} in the native starch to 3443 cm^{-1} . Similarly, the -SO_3 symmetric stretching vibration shifted to 1214 cm^{-1} . Also, the intensity of the -CH_2 group at 2924 cm^{-1} decreased. Additionally, an MB peak (C-S-C-) was observed at 1110 cm^{-1} . From the FTIR spectra, we can conclude that the native starch was modified successfully, with hydroxypropyl sulphonation derivatives obtained and MB adsorbed in HPSS.

Only a few broad peaks were observed in the *Asp. oryzae* FTIR spectra at wavenumbers 3397, 2919, and 1454 cm^{-1} . The broad band stretching at 3397 cm^{-1} is attributed to the existence of the aliphatic and phenolic -OH stretching chain, the major constituent of cellulose-based material inherent in the raw *Asp. oryzae*. The stretching vibrations of the phenolic, carbonyl, amide II, and amide III groups of the lignin are responsible for the band at 1454 cm^{-1} . After adsorption, the functional groups that were responsible for the solute binding shrank considerably while the associated % Transmittance values significantly increased.

3.1.2 Structural properties

X-ray diffraction (XRD) patterns were analyzed on a PAN analytical diffractometer (X'Pert PRO) in continuous scanning mode using a Cu tube (in the reading range of 5 to 80°). The generated X-ray diffraction patterns are presented in Fig. 2a, b. For the HPSS (Fig. 2a, the broad peak which is the signature peak for the amorphous structure of the glucose unit in starch was recorded at $2\theta = 13\text{--}23^\circ$). Also, new sharp peaks appearing at $2\theta = 31.3^\circ$, 45.1° , and 56.3° are due to increased crystallinity occasioned by the existence of the new starch derivatives (HPSS). The loaded HPSS shows different peaks at $2\theta = 14.8^\circ$, 17.6° , 23.1° , and 31.3° which corresponds to the chemical structure of starch derivative. The sharp peaks related to starch derivative (HPSS) decreased

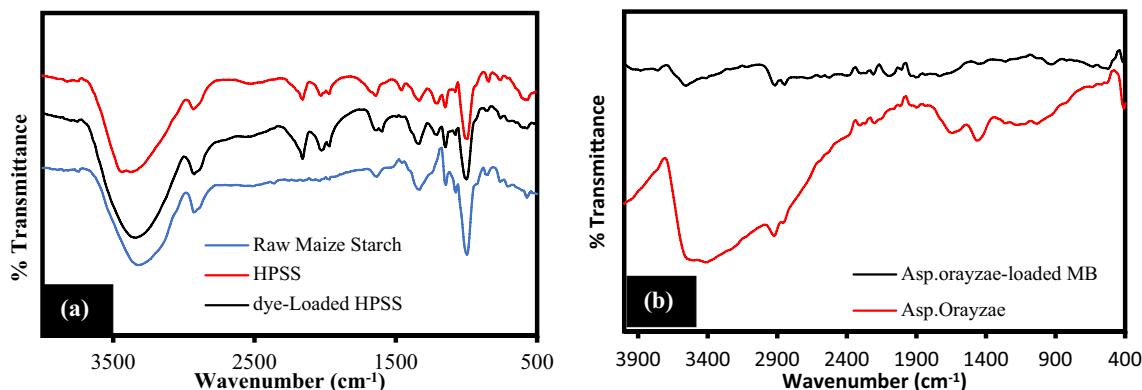


Fig. 1 FTIR spectra of **a** native starch, hydroxypropyl starch sulfate, and hydroxypropyl starch sulfate-loaded methylene blue and **b** raw and loaded *Asp. oryzae*

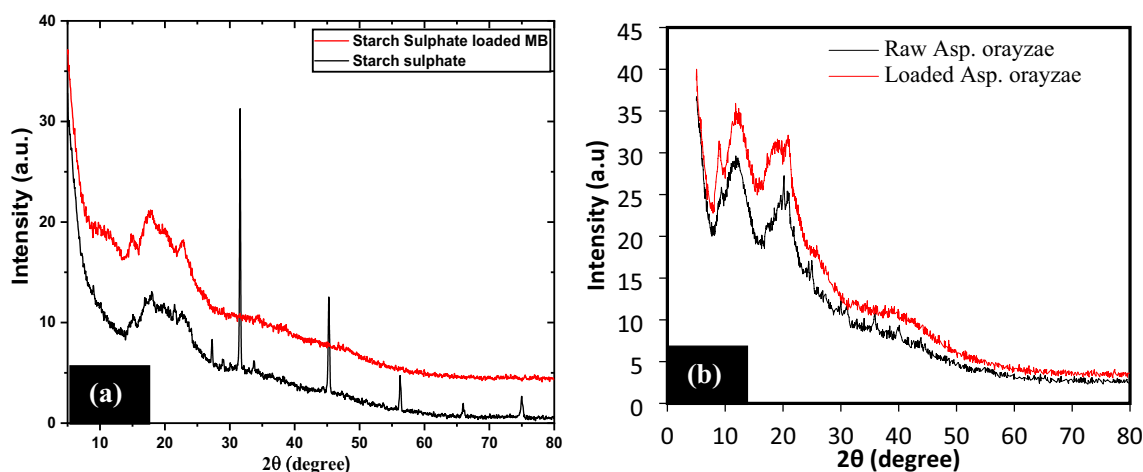


Fig. 2 XRD spectra of the **a** HPSS and loaded HPSS and **b**) raw and dye-loaded *Asp. oryzae*

after adsorption due to the interaction between MB and functional groups of modified starch. This occurred mostly at the upper layer of the HPSS crystalline structure.

Concerning *Asp. oryzae*, two semi-lucid peaks developed around $2\theta = 12.39^\circ$ and 20.23° . It is believed that the semi-lucid peaks are caused by the chitin polysaccharides in the fungal structure. Karthik et al. [21] also noted an analogous semi-lucid peak at $2\theta = 22.64^\circ$ and 41.73° when doing their structural analysis of *Trichoderma harzianum*. The study concluded that the polysaccharides in the fungal cell wall were responsible for the apparent peaks. After noticing a broad peak on *Penicillium* sp. at $2\theta = 20^\circ$, Yu et al. [34] concluded that the fungus adsorbent was amorphous. The dye-loaded samples showed peaks at locations corresponding to the raw sample. This finding shows that the adsorption process did not result in any structural changes.

3.1.3 Surface morphology

Scanning electron microscopy (SEM) micrographs of the samples were analyzed on a scanning electron microscope (model JEOL-JSM-5600) following the standard protocols. The morphological properties of the samples are shown in Fig. 3. From Fig. 3a, a heterogeneous surface due to the presence of polygonal and ellipsoid starch granules was observed. However, the modification completely altered native starch granules' morphology (Fig. 3b). The starch derivatives show sphere-shaped structures with high adhesion morphology between starch granules, and the size of starch granules after chemical modification became smaller than native starch. After the adsorption process, the size and shape of loaded HPSS were completely different compared with native starch and HPSS (Fig. 3c). The loaded HPSS shows irregular and flat heterogenous shapes, with the observation of adherent small MB molecules. The cited

morphological changes were due to the successful chemical modification of starch and the high loading capacity of MB on the starch surface.

Raw *Asp. oryzae* (Fig. 3d) had noticeably crooked surfaces with a dispersion of pores that resembled conduits and waxy ducts. The open channels on the raw *Asp. oryzae* were gone on the post-adsorption micrograph (Fig. 3e). These morphological changes serve as evidence that the solute was successfully bound to the adsorbent surface.

3.1.4 BET surface area

The HPSS showed a BET surface area and pore volume of $93.311 \text{ m}^2/\text{g}$ and $0.066 \text{ cm}^3/\text{g}$, respectively, with an average pore size of 1.924 nm . Therefore, with an average pore size of less than 2 nm , the HPSS is considered a microporous adsorbent. For the *Asp. oryzae*, it has specific surface areas, pore volume, and pore sizes of $25.593 \text{ m}^2/\text{g}$, $0.365 \text{ cm}^3/\text{g}$, and 0.341 nm , respectively. Notably, the surface area and pore radius recorded for the HPSS are higher compared to those of *Asp. oryzae*. Since higher surface area is synonymous with improved adsorption capacity, therefore, HPSS is expected to exhibit higher adsorption capacity than the *Asp. oryzae*. Similarly, the pore radius for both adsorbents is smaller than 2 nm ; hence, they are classified as microporous adsorbents according to the IUPAC [35, 36].

3.2 Process variables studies

3.2.1 Analysis of the adsorbents' pH_{pzc} and effect of solution pH

The point of zero charge was established in this study using the titrimetric method. The generated plot for both

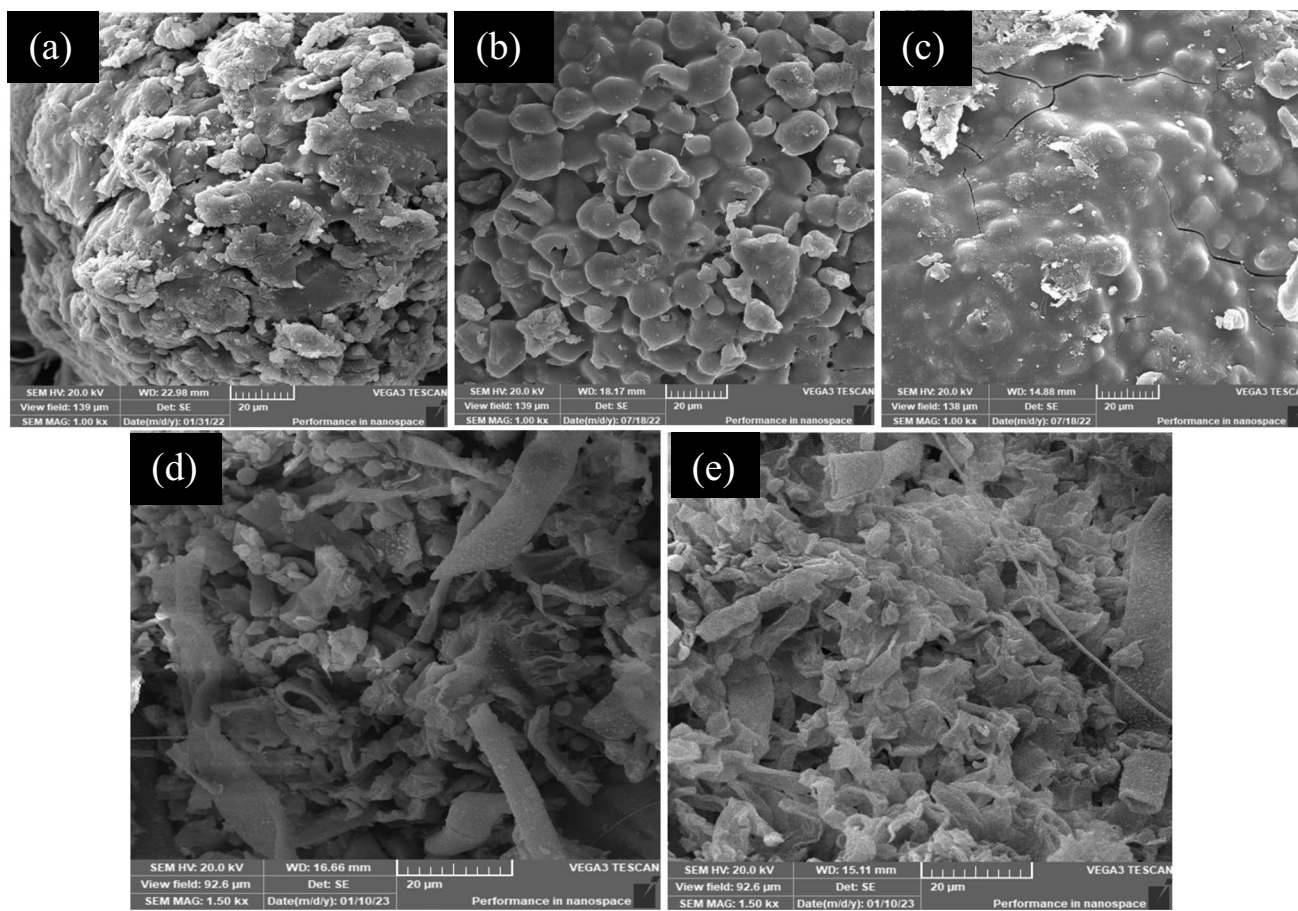
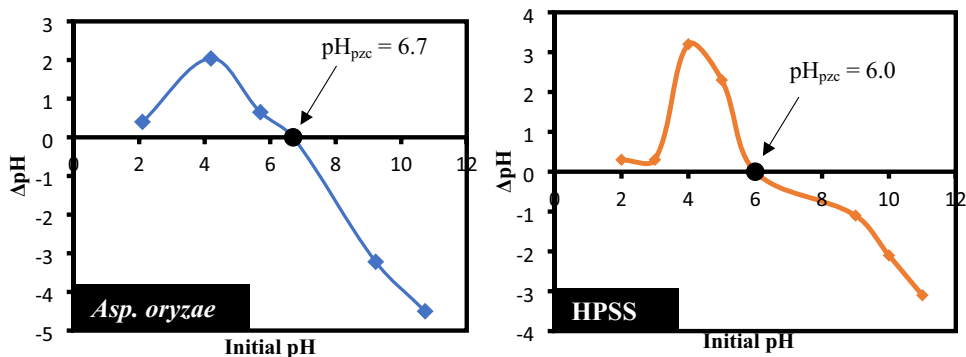


Fig. 3 SEM micrographs of a raw starch, b HPSS, c loaded HPSS, d raw *Asp. oryzae*, and e loaded *Asp. oryzae*

Fig. 4 Plot for the determination of pH_{pzc} of both adsorbents

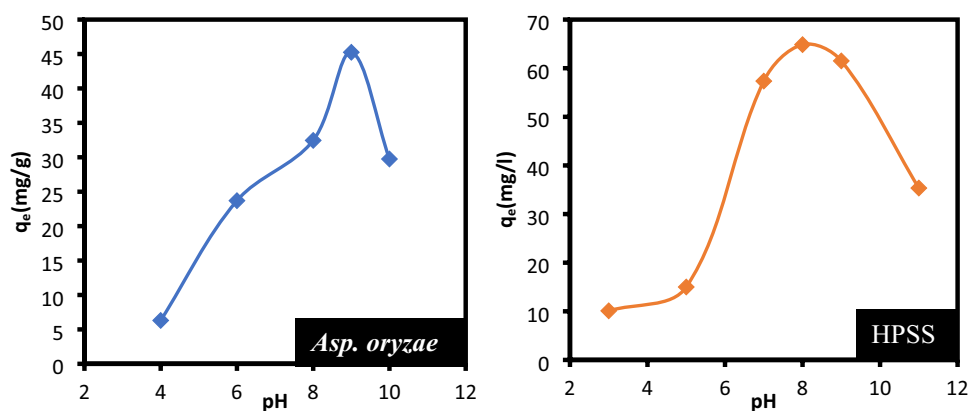


adsorbents is shown in Fig. 4, where it can be seen that the pH_{pzc} for the HPSS and *Asp. oryzae* occur at pH 6.0 and 6.7, respectively. Thus, the adsorption of MB species is expected to occur more favorably when the solution pH is higher than the pH_{pzc} of the respective adsorbents.

Since solution pH sustains a significant effect on the sorption process efficiency, Fig. 5 presents the effect of solution pH on the adsorption capacity. The plot for both adsorbents showed a consistent increase in adsorption capacity as the

solution acidity weakened. This is due to an enhanced attraction between the cationic dye molecules and the progressively deprotonated surface of both adsorbents. However, pH 9.0 and pH 8.0 were recorded as the optimum pH for the adsorption of MB species onto *Asp. oryzae* and HPSS, respectively. Meanwhile, with an increase in solution pH beyond the respective optimums and deep into the alkaline pH ranges, a decrease in adsorption capacity was recorded. This observation is quite uncommon as the optimum

Fig. 5 Plots of the effect of contact time on MB dye adsorption capacity (reaction conditions: MB conc., 20 mg/L; Temp., 30 °C; time, 2 h; adsorbent conc., 0.15 g/L)



adsorption of cationic dye molecules is expected to improve with increased alkalinity. However, this anomaly occurred due to a possible swelling and rupturing of the starch granules and *Asp. oryzae* cells at alkaline conditions [37]. Therefore, the optimum pH for the study was established at pH 9.0 and pH 8.0 for *Asp. oryzae* and HPSS, respectively.

3.2.2 Effect of contact time

The effect of adsorption time as presented in Fig. 6 showed a rapid MB uptake at the onset of adsorption in the case of both adsorbents. Notably, at a constant 20 mg/L concentration, about 61.80 mg/g and 41.35 mg/g of the solute were respectively adsorbed onto the HPSS and *Asp. oryzae* within the first 10 min of adsorption. This is due to the presence of a large number of vacant adsorption sites and the shortened diffusion path phenomenon obtainable at the early stages

of the adsorption process. Due to active site saturation, the adsorption rate progressively abated after the first 10 min of contact time. This is such that only about 4.30 mg/g of HPSS and 3.65 mg/g of *Asp. oryzae* was additionally adsorbed afterwards until equilibrium was finally attained at 60 min. Furthermore, at the optimum time of 60 min, HPSS recorded an adsorption capacity of 66.13 mg/g, and this value is quite larger than the 45.0 mg/g recorded by *Asp. oryzae*. This finding shows that the surface area difference between both adsorbents also had a significant impact on their respective adsorption capacity since HPSS exhibit a larger surface area.

3.2.3 Effect of adsorbent dose

The effect of the variation of the adsorbent concentration on the adsorption capacity is presented in Fig. 7. Accordingly, the plot shows a decrease in the adsorption capacity

Fig. 6 Plots of the effect of contact time on MB dye adsorption capacity [reaction conditions: MB conc., 20 mg/L; Temp., 30 °C; time, 2 h; adsorbent conc., 0.15 g/L; pH 8.0–9.0]

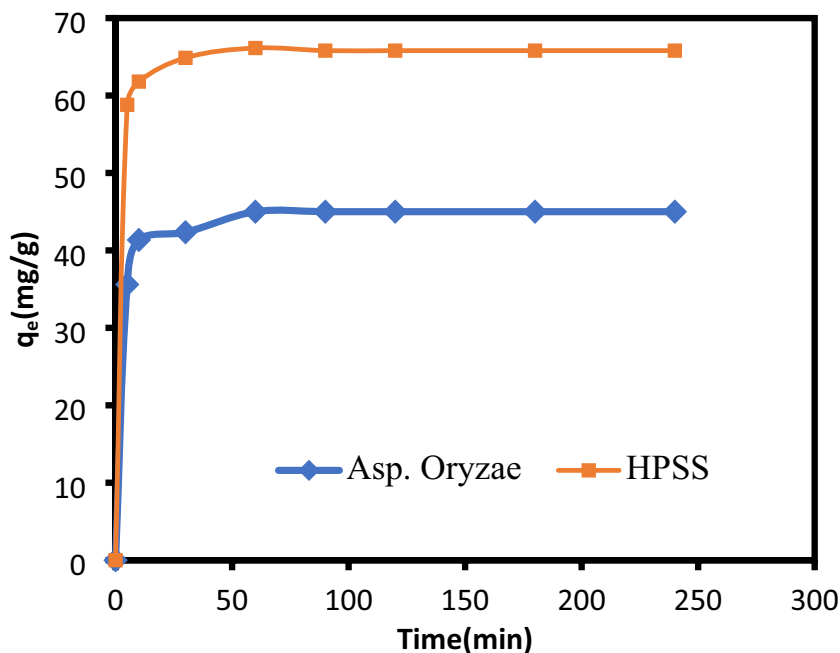
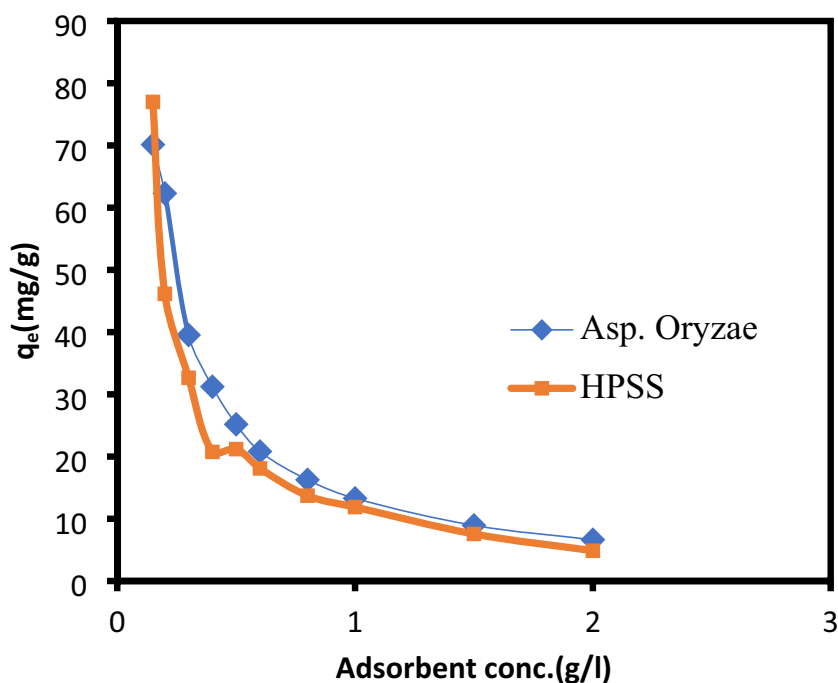


Fig. 7 Plots of the effect of adsorbent concentration on MB dye adsorption capacity [reaction conditions: MB conc., 20 mg/L; Temp., 30 °C; time, 2 h]



of both adsorbents as the adsorbent concentration increased. Specifically, at least the adsorbent concentration studied (0.15 g/L), HPSS, and *Asp. oryzae* respectively adsorbed 77.0 and 70.0 mg/g of MB species. Conversely, when the adsorbent concentration was raised to 2.0 g/L, the adsorption capacities were reduced to 4.87 and 6.63 mg/g for HPSS and *Asp. oryzae*, respectively. This observation is attributed to the disproportionality occasioned by the introduction of a greater number of active sites via the increase in adsorbent dosage even at initial adsorbate concentration. Such development triggers a progressive unsaturation of these active sites, as the amount of MB species adsorbed per gram of adsorbent drops. Also, the probable particle agglomeration and clogging at high dosages could limit the surface area of the respective adsorbents and by extension, their overall adsorption capacity. A similar occurrence of a reduction in adsorption density with an increase in the adsorbent dose was reported by Aljeboree et al. [38] during the adsorption of maxilon blue GRL and direct yellow DY 12 onto coconut husk-activated carbon. The authors claim that the incidences of sustained unsaturation in the face of an increase in the number of available adsorptions was the primary cause of this development.

3.2.4 Effect of temperature

The adsorption process is significantly impacted by temperature variation since it can change the adsorbates' kinetic energy and physicochemical composition [39]. Figure 8 presents the relationship between temperature and adsorption

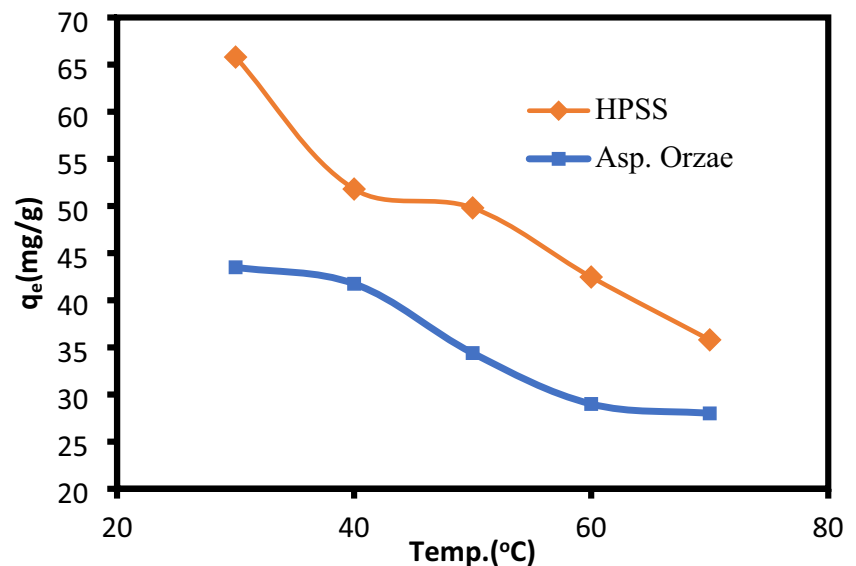
capacity for both adsorbents. Consequently, a consistent adsorption capacity decrease was observed with temperature rise. For instance, the adsorption capacity decreased from 66.50 to 37.0 mg/g (for HPSS) and from 43.50 to 28.00 mg/g (for *Asp. oryzae*) as the temperature increased from 30 to 70 °C. This observation suggests the occurrence of an exothermic process where the electrostatic properties of the adsorbents are temperature-dependent. Also, a physisorption interaction which weakens with increasing temperature is postulated.

3.3 Adsorption modelling

3.3.1 Isotherm studies

The equilibrium data was further described using the dedicated models presented in Eqs. (3)–(10). The generated isotherm model parameters for both adsorbents are presented in Table 3, while the plots for 2-parameter and 3-parameter models are presented in Figs. 9 and 10, respectively. As earlier stated (Section 2.4), the model of best fit is determined based on the magnitude of the SNE value. These SNE values are more appropriate compared to the coefficient of determination (R^2) for evaluating the nonlinear models. Generally, the lower the SNE value, the better the model's description. The number of adsorption model parameters has been shown to have a significant impact on the models' fitting ability. Therefore, the isotherm models are generally groups based on the number of model parameters and the associated discussion follows a similar pattern.

Fig. 8 Plots of the effect of temperature on MB dye adsorption capacity [reaction conditions: MB conc., 20 mg/L; adsorbent conc., 0.15 g/L; time, 2 h; pH 8.0–9.0]



The Freundlich isotherm model with the lowest SNE values of 1.48 and 1.96 for HPSS and *Asp. oryzae* is regarded as the best fit for 2-parameter models (Fig. 9). The Freundlich isotherm predicts multi-layer adsorption with an equilibrium coverage proportion of roughly 50% on heterogeneous surfaces [27, 40]. According to the existing hypothesis about the range of $1/n$ -values and how they relate to the adsorption system [40], the $1/n$ -values obtained in Table 3 are greater than zero but less than unity, thus indicating that the adsorption is favorable. Having identified the best fit, the significance of the magnitude of the constants generated for the other 2-parameter isotherm model to the present adsorption system is further elucidated. The Langmuir K_L constant values of 1.3 and 5.43 L/g were obtained respectively for HPSS and *Asp. oryzae* indicates a reasonable adsorbent-adsorbate interaction [41, 42]. Also, the Langmuir favorability index (R_L) value of 0.02 (for HPSS) and 0.07 (for *Asp. oryzae*) indicates favorable adsorption processes [40, 43]. Also, the Freundlich maximum adsorption capacity parameter (k_F) is reasonably larger than unity for both adsorbents.

For the 3-parameter models (Fig. 8), the Khan isotherm model with the lowest SNE value of 1.43 and 2.11 for HPSS and *Asp. oryzae* is considered the best fit. The magnitude of the models' exponent (a_K) which indicates the nature of the adsorptive interaction is less than unity for both adsorbents and thus suggests a heterogeneous adsorption process [27]. Upon further consideration of the parametric implication of other models to the present adsorption system, it is well known that the Sip model respectively reduces to the Freundlich and Langmuir model at β_S -value equal to 1 and 0. However, the β_S -value obtained for both adsorbents could be approximated to unity, hence, suggesting the predominance of Freundlich. The cooperative adsorption index for the Hill model (n_H) was recorded as 0.59 (for HPSS) and 0.74 (for

Asp. oryzae), thus indicating negative cooperativities. Consequently, the affinity of the respective adsorbents for MB species is progressively limited as the adsorption duration extends [44, 45]. The “ t ” parameter of the Toth model provides insight into the heterogeneity of the adsorption system. Thus, a given adsorption system is considered heterogeneous when (t) does not equal unity [46]. On this basis, the adsorption system for both adsorbents is heterogeneous.

3.3.2 Kinetic studies

The MB dye adsorption onto HPSS and *Asp. oryzae* at an initial concentration of 20 mg/L and optimum adsorbent dosage was investigated using classical kinetic models whose theoretical background and mathematical expressions are presented in Section 2.3 and Eqs. (11)–(13). The results from the kinetics modelling are presented in Table 4 and Fig. 11. Generally, all the kinetic models gave a satisfactory R^2 value ($R^2 > 0.9$). However, taking the magnitude of SNE value as the basis for determining the kinetic model of best fit, just as was the case in isotherm studies, the Elovich and PFO models are considered the best fit for HPSS and *Asp. oryzae*. The Elovich model signifies the chemisorption of MB onto energetically heterogeneous sorption sites, while the PFO model suggests the predominance of physisorption via interfacial diffusion. An overview of the implication of the different kinetic model parameters shows that Elovich's initial adsorption rate (α) value was much greater than the desorption constant (β) for both adsorbents, thus indicating a stable uptake process. Also, the k_2 -value recorded in Table 4 was much lower than the k_1 -value and implies faster second-order rate sorption.

The linear form of the intraparticle diffusion models (Eq. 14) and the associated plots (Fig. 12) was applied to

Table 3 Isotherm model parameters

Adsorbents	2-parameter isotherm models	
HPSS	Langmuir	Freundlich
	$q_{max} = 52.41$	$n_F = 1.73$
	$K_L = 1.3$	$1/n_F = 0.58$
	$R_L = 0.02$	$K_F = 2.00$
	$R^2 = 0.931$	$R^2 = 0.991$
	SNE = 2.43	SNE = 1.48
	3-parameter isotherm models	
	Khan	Redlich-P
	$q_{max} = 0.17$	$K_R = 1.57$
	$a_K = 0.46$	$\alpha_R = -0.38$
$b_K = 117.38$	$g = 0.22$	
$R^2 = 0.992$	$R^2 = 0.981$	
SNE = 1.43	SNE = 1.54	
2-parameter isotherm models		
Langmuir	Freundlich	
$q_{max} = 37.26$	$n_F = 1.35$	
$K_L = 5.43$	$1/n_F = 0.74$	
$R_L = 0.07$	$K_F = 5.92$	
$R^2 = 0.987$	$R^2 = 0.990$	
SNE = 2.08	SNE = 1.96	
3-parameter isotherm models		
Khan	Redlich-P	
$q_{max} = 0.22$	$K_R = 2.22$	
$a_K = 0.28$	$\alpha_R = -0.73$	
$b_K = 103.13$	$g = 0.10$	
$R^2 = 0.991$	$R^2 = 0.994$	
SNE = 2.11	SNE = 2.81	
Asp. oryzae	2-parameter isotherm models	
	Langmuir	Freundlich
	$q_{max} = 30.02$	$n_F = 1.73$
	$b_T = 2000.0$	$1/n_F = 0.58$
	$R^2 = 0.895$	$K_F = 2.00$
	SNE = 1.79	SNE = 1.48
	3-parameter isotherm models	
	Toth	Sips
	$k_T = 1.99$	$K_S = 2.00$
	$\alpha_T = 0.10$	$\alpha_S = -0.01$
$1/t = 0.42$	$\beta_S = 0.56$	
$R^2 = 0.991$	$R^2 = 0.991$	
SNE = 1.51	SNE = 1.49	
2-parameter isotherm models		
Temkin	Freundlich	
$A_T = 32.78$	$n_F = 1.35$	
$b_T = 1567.94$	$1/n_F = 0.74$	
$R^2 = 0.910$	$K_F = 5.92$	
SNE = 2.13	$R^2 = 0.990$	
3-parameter isotherm models		
Toth	Sips	
$k_T = 6.11$	$K_S = 5.86$	
$\alpha_T = 0.09$	$\alpha_S = -0.01$	
$1/t = 0.27$	$\beta_S = 0.72$	
$R^2 = 0.990$	$R^2 = 0.990$	
SNE = 1.97	SNE = 1.97	
2-parameter isotherm models		
Hill	Hill	
$q_{SH} = 200$	$q_{SH} = 2000$	
$n_H = 0.59$	$n_H = 0.74$	
$k_H = 1021.49$	$k_H = 336.56$	
$R^2 = 0.991$	$R^2 = 0.990$	
SNE = 1.49	SNE = 1.96	

Fig. 9 The plots of 2-parameter isotherm models for *Asp. oryzae* and HPSS [reaction conditions: adsorbent conc., 0.15 g/L; pH, 8; contact time 2 h; Temp., 30 °C]

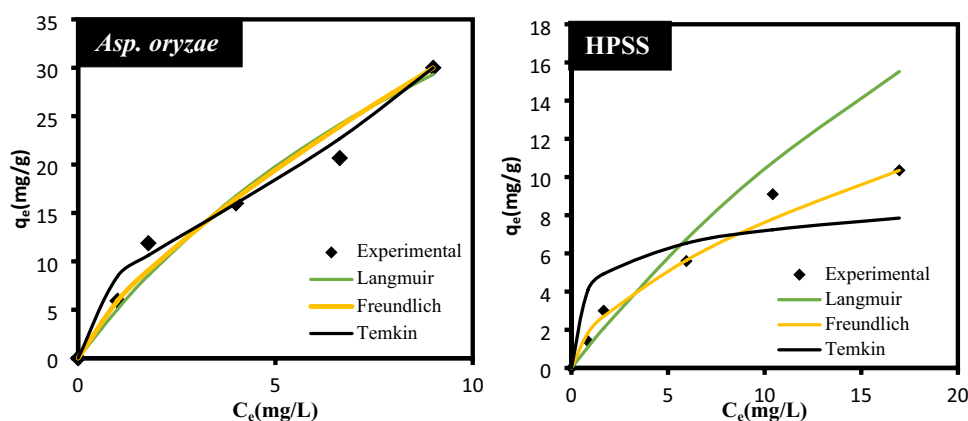


Fig. 10 The plots of 3-parameter isotherm models for *Asp. oryzae* and HPSS [reaction conditions: adsorbent conc., 0.15 g/L; pH, 8; contact time 2 h; temperature, 30 °C]

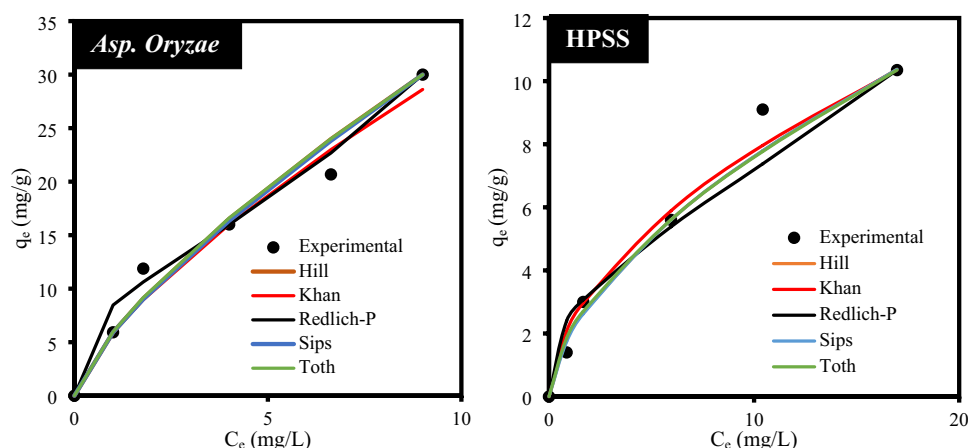


Table 4 Kinetic model parameters

	PFO	PSO	Elovich	Intraparticle
<i>Asp. oryzae</i>	$q_{e, cal} = 45.00$	$q_{e, cal} = 46.49$	$\alpha = 842.63$	$K_{id} = 1.05$
	$k_1 = 0.19$	$k_2 = 0.007$	$\beta = 0.21$	$C = 35.00$
	$R^2 = 0.998$	$R^2 = 0.999$	$R^2 = 0.998$	$R^2 = 0.998$
	SNE = 1.60	SNE = 3.17	SNE = 1.77	
HPSS	$q_{e, cal} = 65.79$	$q_{e, cal} = 65.54$	$\alpha = 200$	$K_{id} = 0.19$
	$k_1 = 1.45$	$k_2 = 0.02$	$\beta = 0.16$	$C = 63.31$
	$R^2 = 0.999$	$R^2 = 0.999$	$R^2 = 0.988$	$R^2 = 0.998$
	SNE = 1.51	SNE = 3.76	SNE = 1.19	

elucidate the rate-limiting step during MB removal and the model recorded good R^2 -values for both adsorbents. This is an indication of the occurrence of film diffusion characteristics during the MB adsorption. Similarly, the fact that the intercept (c-parameter) of the intraparticle diffusion model is far greater than zero corroborates the earlier assertion for the predominance of the film diffusion mechanism [47, 48].

3.4 Plausible adsorption mechanism

The efficient adsorption of MB onto HPSS and *Asp. oryzae* was mainly due to electrostatic interactions and hydrogen bonding mechanisms as shown in Scheme 2. For both adsorbents, the post-adsorption FTIR spectra (Fig. 1) showed a general increase in the % transmittance of the main peaks, particularly the hydroxyl, amino, and sulfate groups. Based on the pH studies, the hydrogen bond donor and acceptor groups (oxygen- and nitrogen-based groups) in the HPSS can also form hydrogen bonds with dye molecules (Scheme 2a). Specifically, the $-\text{SO}_3$ groups on the HPSS shared some electrostatic affinity with the MB dye cationic center (N^+ backbone), while a hydrogen bond is formed between the hydroxyl groups of the starch and N^+ backbone of the MB dye. Also, the post-adsorption XRD spectra showed a decrease in the sharp crystalline peaks of HPSS. This is attributed to the adsorption of MB dye on the upper layer of the crystalline structure of the HPSS via electrostatic interaction and hydrogen bond formation. Additionally, the binding of MB species was significantly influenced by the nitrogen- and oxygen-containing groups

Fig. 11 The plots of the PFO, PSO, and Elovich models for *Asp. oryzae* and HPSS [reaction conditions: MB conc., 20 mg/L; adsorbent conc. 0.15 g/L; pH, 8; temp., 30 °C]

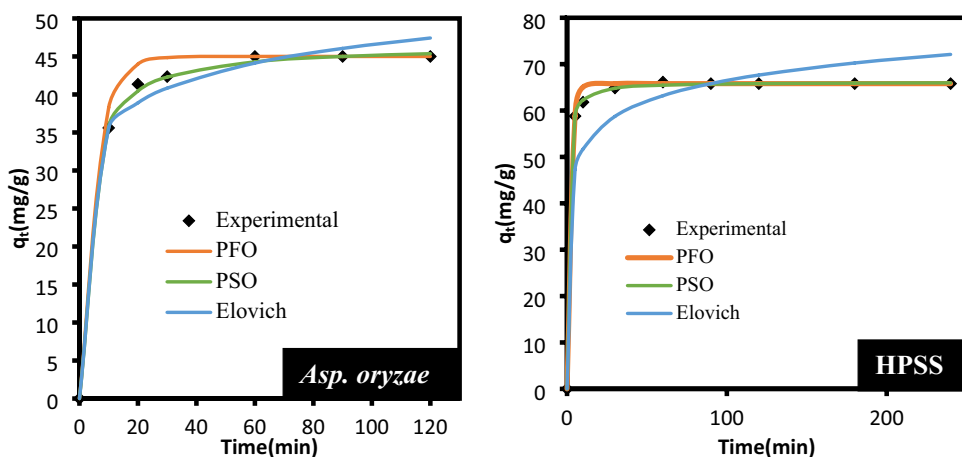
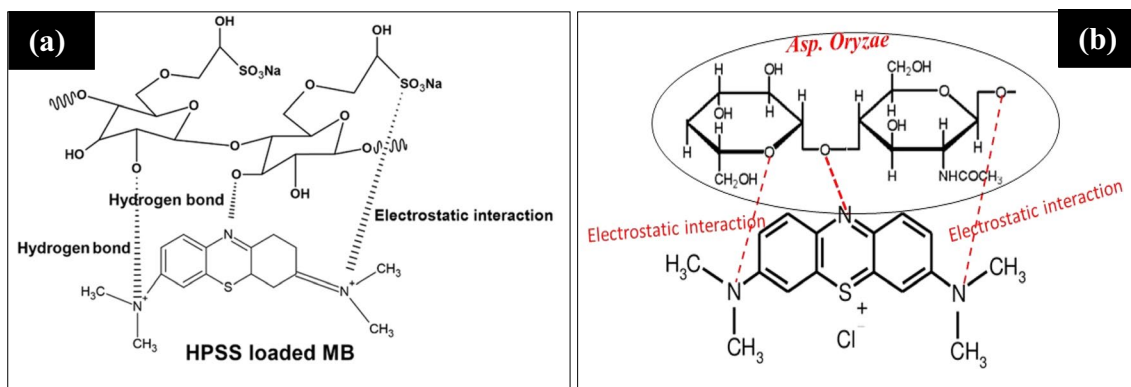
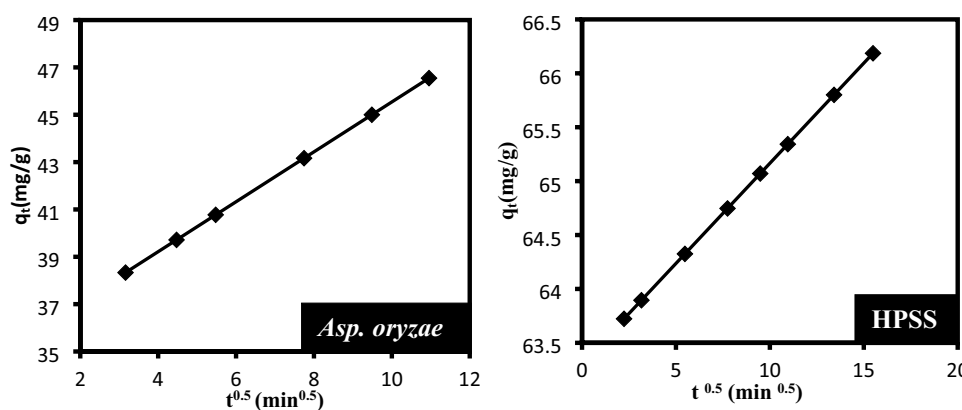


Fig. 12 The intraparticle diffusion model plots for *Asp. oryzae* and HPSS [reaction conditions: MB conc., 20 mg/L; adsorbent conc. 0.15 g/L; pH, 8; temp., 30 °C]



Scheme 2 Proposed mechanism for MB sorption onto **a** HPSS and **b** *Asp. oryzae*

on the *Asp. oryzae*. These functional groups attracted the charged adsorbate species via an electrostatic interaction mechanism, as depicted in Scheme 2b.

Table 5 displays a comparison of the MB adsorptive performance of different fungal- and starch-based adsorbents to those of the adsorbents utilized in this study. From

the presented data, it is observed that the adsorption performance recorded in this study is well-situated among the previously published works.

Table 5 Comparison of the MB adsorptive performance of different adsorbents

Adsorbent	Process variable				q_{\max} (mg/g)	Ref
	pH	Time (min)	Adsorbent dose (g/L)	Initial conc (mg/L)		
<i>Rhizopus oryzae</i>	7.0	60	4.0	50	8.3	[49]
<i>Penicillium glabrum</i>	8.2	180	0.33	10	16.7	[50]
<i>Aspergillus carbonarius</i>	8.2	180	0.33	10	21.9	[50]
<i>Asp. oryzae</i>	8.0–9.0	120	0.2	20	37.3	Present study
<i>A. fabrum</i>	11	60	1.0	200	91.0	[51]
HPSS	8.0–9.0	120	0.2	20	52.41	Present study
<i>Agaricus bisporus</i>	8.0	240	0.05	50	239.8	[52]
Starch composite	5.5	30.0	0.15	40	604.0	[53]
Starch/rice husk hydrogel	5.0	60.0	0.5	2000	1906.3	[16]

3.5 Cost estimation for producing 1 kg of the adsorbent

When choosing a treatment approach for pollutant removal, cost analysis frequently helps [54]. Because the cost of the adsorbent being utilized is a major determinant of adsorption cost, doing a thorough cost analysis is crucial when choosing an adsorbent [55]. The most common adsorbent used in the water treatment process at the moment is commercial activated carbon, yet it is highly costly. Because of this, activated carbon adsorbent is frequently not a sustainable economic option for treating wastewater containing dyes. Therefore, such costly material is out of reach for small and medium-sized businesses in developing nations. Therefore, there is a great demand for an inexpensive adsorbent that is readily available in nature, low cost, and just as effective as activated carbon. The present work is based on the synthesis and dye adsorption application of hydroxypropyl starch sulfate (HPSS)

and *Aspergillus oryzae* (*Asp. oryzae*). After a detailed evaluation of the cost analyses as shown in Table 6, it is observed that the cost for producing 1 kg of each of the *Asp. oryzae* and HPSS adsorbents are USD 1.54 and USD 37.95, respectively. Notably, the combined cost of both adsorbents is far lower when compared to the cost per kilogram of commercial activated carbon, which is about USD 172.96 per kg [56]. Thus, the *Asp. oryzae* and HPSS are both considered effective and low-cost dye adsorbents.

4 Conclusion

This work successfully generated hydroxypropyl starch sulfate (HPSS) and *Aspergillus oryzae* (*Asp. oryzae*) biomass and examined their ability to adsorb methylene blue (MB) dye. By adjusting several process variables, including the initial dye concentration, temperature, time, solution pH, and adsorbent dose, the adsorptive qualities of

Table 6 Estimated cost of producing 1 kg of the respective adsorbents

S/N	Material	Number of units	Net price (USD)
(a) Estimate cost per kg of <i>Asp. oryzae</i>			
1	Potato dextrose broth (PDB)	200 g	0.64
2	Energy cost for drying (80 °C, 2 h)	1.00 kWh	0.83
	Net price	-	1.47
	Other overhead costs (5% of the net cost)	-	0.07
		Total cost [net + overhead cost]	1.54
(b) Estimate cost per kg of HPSS			
1	Epichlorohydrin	300 g	15.58
2	Sodium sulfite	300 g	17.53
3	Sodium hydroxide	187.5 g	1.73
4	Maize starch	1100 g	1.30
	Net price	-	36.14
	Other overhead costs (5% of the net cost)	-	1.81
		Total cost [net + overhead cost]	37.95

both adsorbents were efficiently studied in batch mode. To further clarify each adsorbent's unique functional, textural, and morphological characteristics, a thorough analysis of the materials using the FTIR, XRD, SEM, EDX, and BET surface area studies was also carried out. Based on the result of the pore distribution analyses, both adsorbents are categorized as micro-mesoporous adsorbents since their pore radii are less than 2 nm. The study's isotherm models and related discussions were categorized according to the number of parameters in each model. The isotherm modelling followed the Freundlich (for 2-parameter models studied) and the Khan (for 3-parameter models studied). Similarly, PFO and Elovich models respectively emerged as the best-fit kinetic model for *Asp. oryzae* and HPSS. Notably, the nitrogen- and oxygen-containing groups on the *Asp. oryzae* had a substantial impact on the binding of MB species. Through an electrostatic interaction mechanism, these functional groups attracted the charged adsorbate species. The MB dye's cationic center (N^+ backbone) and the $-SO_3$ groups on the HPSS also shared some electrostatic affinity, coupled with a probable formation of hydrogen bond between the hydroxyl groups of the starch and the N^+ backbone of the MB dye.

Author contribution AH: project administration, data curation, supervision, experimentation, conceptualization, writing—review and editing.

COA: conceptualization, data curation, writing—original draft, writing—review and editing.

LAM: investigation, methodology, data analysis and provided critical feedback on the manuscript draft.

AMA: investigation, methodology, data analysis and provided critical feedback on the manuscript draft.

AAA: investigation, methodology, data analysis and provided critical feedback on the manuscript draft.

All authors have read and approved the final manuscript.

Funding Open access funding provided by The Science, Technology & Innovation Funding Authority (STDF) in cooperation with The Egyptian Knowledge Bank (EKB).

Data availability All data generated or analyzed during this study are included in this published article.

Declarations

Ethical approval Not applicable.

Competing interests The authors declare no competing interests.

Open Access This article is licensed under a Creative Commons Attribution 4.0 International License, which permits use, sharing, adaptation, distribution and reproduction in any medium or format, as long as you give appropriate credit to the original author(s) and the source, provide a link to the Creative Commons licence, and indicate if changes were made. The images or other third party material in this article are included in the article's Creative Commons licence, unless indicated otherwise in a credit line to the material. If material is not included in

the article's Creative Commons licence and your intended use is not permitted by statutory regulation or exceeds the permitted use, you will need to obtain permission directly from the copyright holder. To view a copy of this licence, visit <http://creativecommons.org/licenses/by/4.0/>.

References

- Kuang Y, Zhang X, Zhou S (2020) Adsorption of methylene blue in water onto activated carbon by surfactant modification. *Water* 12(2):587
- Khan I, Saeed K, Zekker I, Zhang B, Hendi AH, Ahmad A, Ahmad S, Zada N, Ahmad H, Shah LA (2022) Review on methylene blue: its properties, uses, toxicity and photodegradation. *Water* 14(2):242
- Din MI, Khalid R, Najeeb J, Hussain Z (2021) Fundamentals and photocatalysis of methylene blue dye using various nanocatalytic assemblies—a critical review. *J Clean Prod* 298:126567
- Alkaykh S, Mbarek A, Ali-Shattle EE (2020) Photocatalytic degradation of methylene blue dye in aqueous solution by MnTiO₃ nanoparticles under sunlight irradiation. *Heliyon* 6(4):e03663
- Mian MM, Liu G (2019) Sewage sludge-derived TiO₂/Fe/Fe₃C-biochar composite as an efficient heterogeneous catalyst for degradation of methylene blue. *Chemosphere* 215:101–114
- Jorge N, Teixeira AR, Marchão L, Tavares PB, Lucas MS, Peres JA (2022) Removal of methylene blue from aqueous solution by application of plant-based coagulants. *Eng Proc* 19(1):38
- Ihaddaden S, Aberkane D, Boukerroui A, Robert D (2022) Removal of methylene blue (basic dye) by coagulation-flocculation with biomaterials (bentonite and *Opuntia ficus indica*). *J Water Process Eng* 49:102952
- Wen D, Li W, Lv J, Qiang Z, Li M (2020) Methylene blue degradation by the VUV/UV/persulfate process: effect of pH on the roles of photolysis and oxidation. *J Hazard Mater* 391:121855
- Nguyen DH, Tran HN, Chao H-P, Lin C-C (2019) Effect of nitric acid oxidation on the surface of hydrochars to sorb methylene blue: an adsorption mechanism comparison. *Adsorpt Sci Technol* 37(7–8):607–622
- Sahu A, Dosi R, Kwiatkowski C, Schmal S, Poler JC (2023) Advanced polymeric nanocomposite membranes for water and wastewater treatment: a comprehensive review. *Polymers* 15(3):540
- Sahu A, Blackburn K, Durkin K, Eldred TB, Johnson BR, Sheikh R, Amburgey JE, Poler JC (2018) Green synthesis of nanoscale anion exchange resin for sustainable water purification. *Environ Sci: Water Res Technol* 4(10):1685–1694
- Yao X, Ji L, Guo J, Ge S, Lu W, Cai L, Wang Y, Song W, Zhang H (2020) Magnetic activated biochar nanocomposites derived from wakame and its application in methylene blue adsorption. *Biores Technol* 302:122842
- Alver E, Metin AÜ, Brouers F (2020) Methylene blue adsorption on magnetic alginate/rice husk bio-composite. *Int J Biol Macromol* 154:104–113
- Chen R, Zhang Y, Shen L, Wang X, Chen J, Ma A, Jiang W (2015) Lead (II) and methylene blue removal using a fully biodegradable hydrogel based on starch immobilized humic acid. *Chem Eng J* 268:348–355
- Chen L, Zhu Y, Cui Y, Dai R, Shan Z, Chen H (2021) Fabrication of starch-based high-performance adsorptive hydrogels using a novel effective pretreatment and adsorption for cationic methylene blue dye: behavior and mechanism. *Chem Eng J* 405:126953

16. de Azevedo AC, Vaz MG, Gomes RF, Pereira AG, Fajardo AR, Rodrigues FH (2017) Starch/rice husk ash based superabsorbent composite: high methylene blue removal efficiency. *Iran Polym J* 26(2):93–105
17. Mahmoodi-Babolan N, Heydari A, Nematollahzadeh A (2019) Removal of methylene blue via bioinspired catecholamine/starch superadsorbent and the efficiency prediction by response surface methodology and artificial neural network-particle swarm optimization. *Biores Technol* 294:122084
18. Junlapong K, Maijan P, Chaibundit C, Chantarak S (2020) Effective adsorption of methylene blue by biodegradable superabsorbent cassava starch-based hydrogel. *Int J Biol Macromol* 158:258–264
19. Chen QJ, Zheng XM, Zhou LL, Zhang YF (2019) Adsorption of Cu (II) and methylene blue by succinylated starch nanocrystals. *Starch-Stärke* 71(7–8):1800266
20. Munagapati VS, Wen H-Y, Wen J-C, Gutha Y, Tian Z, Reddy GM, Garcia JR (2021) Anionic congo red dye removal from aqueous medium using Turkey tail (*Trametes versicolor*) fungal biomass: adsorption kinetics, isotherms, thermodynamics, reusability, and characterization. *J Dispersion Sci Technol* 42(12):1785–1798
21. Karthik V, Kumar PS, Harsha Vardhan K, Saravanan K, Nithyakala N (2022) Adsorptive behaviour of surface tailored fungal biomass for the elimination of toxic dye from wastewater. *Int J Environ Anal Chem* 102(16):4710–4725
22. Saravanan A, Karishma S, Kumar PS, Varjani S, Yaashikaa P, Jeevanantham S, Ramamurthy R, Reshma B (2021) Simultaneous removal of Cu (II) and reactive green 6 dye from wastewater using immobilized mixed fungal biomass and its recovery. *Chemosphere* 271:129519
23. Shakya M, Sharma P, Meryem SS, Mahmood Q, Kumar A (2016) Heavy metal removal from industrial wastewater using fungi: uptake mechanism and biochemical aspects. *J Environ Eng* 142(9):C6015001
24. Hebeish AA, Aly AA (2014) Synthesis, characterization and utilization of starch hydroxypropyl sulphate for cationic dye removal. *Int J Org Chem* 4(03):208
25. Mohamed L, Aniagor CO, Aly A, Hashem A (2023) Removal of chromium (VI) and acid orange 142 dye from contaminated wastewater using bio-waste mycelium of *Aspergillus ustus*: extraction, isotherms and kinetics studies. *Water Conserv Sci Eng* 8(1):31
26. Langmuir I (1918) The adsorption of gases on plane surfaces of glass, mica and platinum. *J Am Chem Soc* 40(9):1361–1403
27. Al-Ghouti MA, Da'ana DA (2020) Guidelines for the use and interpretation of adsorption isotherm models: a review. *J Hazard Mater* 393:122383
28. Kalam S, Abu-Khamsin SA, Kamal MS, Patil S (2021) Surfactant adsorption isotherms: a review. *ACS Omega* 6(48):32342–32348
29. Ho Y, Porter J, McKay G (2002) Equilibrium isotherm studies for the sorption of divalent metal ions onto peat: copper, nickel and lead single component systems. *Water Air Soil Pollut* 141(1–4):1–33
30. An B (2020) Cu (II) and As (V) adsorption kinetic characteristic of the multifunctional amino groups in chitosan. *Processes* 8(9):1194
31. Ho Y-S, McKay G (2003) Sorption of dyes and copper ions onto biosorbents. *Process Biochem* 38(7):1047–1061
32. Simonin J-P, Bouté J (2016) Intraparticle diffusion-adsorption model to describe liquid/solid adsorption kinetics. *Rev Mex Ing Quím* 15(1):161–173
33. Hashem A, Aniagor CO, Nasr MF, Abou-Okeil A (2021) Efficacy of treated sodium alginate and activated carbon fibre for Pb (II) adsorption. *Int J Biol Macromol* 176:201–216
34. Yu D, Bo B, Yunhua H (2013) Fabrication of TiO₂@ yeast-carbon hybrid composites with the raspberry-like structure and their synergistic adsorption-photocatalysis performance. *J Nanomater* 2013:20–20
35. Zdravkov B, Čermák J, Šefara M, Janků J (2007) Pore classification in the characterization of porous materials: a perspective. *Open Chem* 5(2):385–395
36. Mays T (2007) A new classification of pore sizes. *Stud Surface Sci Catal* 160(Characterization of Porous Solids VII):57–62
37. Chou S, Li B, Tan H, Zhang W, Zang Z, Cui H, Wang H, Zhang S, Meng X (2020) The effect of pH on the chemical and structural interactions between apple polyphenol and starch derived from rice and maize. *Food Sci Nutr* 8(9):5026–5035
38. Aljeboree AM, Alshirifi AN, Alkaim AF (2017) Kinetics and equilibrium study for the adsorption of textile dyes on coconut shell activated carbon. *Arab J Chem* 10:S3381–S3393
39. Ebelegi AN, Ayawei N, Wankasi D (2020) Interpretation of adsorption thermodynamics and kinetics. *Open J Phys Chem* 10(03):166–182
40. Wang J, Guo X (2020) Adsorption isotherm models: classification, physical meaning, application and solving method. *Chemosphere* 258:127279
41. Alkurdi SS, Al-Juboori RA, Bundschuh J, Bowtell L, Marchuk A (2021) Inorganic arsenic species removal from water using bone char: a detailed study on adsorption kinetic and isotherm models using error functions analysis. *J Hazard Mater* 405:124112
42. Azizian S, Haerifar M, Basiri-Parsa J (2007) Extended geometric method: a simple approach to derive adsorption rate constants of Langmuir-Freundlich kinetics. *Chemosphere* 68(11):2040–2046
43. Chowdhury S, Saha P (2010) Sea shell powder as a new adsorbent to remove Basic Green 4 (Malachite Green) from aqueous solutions: equilibrium, kinetic and thermodynamic studies. *Chem Eng J* 164(1):168–177
44. Majd MM, Kordzadeh-Kermani V, Ghalandari V, Askari A, Sillanpää M (2021) Adsorption isotherm models: a comprehensive and systematic review (2010–2020). *Sci Total Environ* 812:151334
45. Chen X, Hossain MF, Duan C, Lu J, Tsang YF, Islam MS, Zhou Y (2022) Isotherm models for adsorption of heavy metals from water-a review. *Chemosphere* 307:135545
46. Podder M, Majumder C (2019) Bacteria immobilization on neem leaves/MnFe₂O₄ composite surface for removal of As (III) and As (V) from wastewater. *Arab J Chem* 12(8):3263–3288
47. Mall ID, Srivastava VC, Agarwal NK, Mishra IM (2005) Adsorptive removal of malachite green dye from aqueous solution by bagasse fly ash and activated carbon-kinetic study and equilibrium isotherm analyses. *Colloids Surf, A* 264(1–3):17–28
48. Hashem A, Aniagor CO, Abdel-Halim E, Amr A, Farag S, Aly A (2022) Instrumental characteristics and acid blue 193 dye sorption properties of novel lupine seed powder. *Clean Chem Eng* 2:100011
49. Dey MD, Shukla R, Bordoloi NK, Doley R, Mukhopadhyay R (2015) Mechanism of adsorptive removal of methylene blue using dried biomass of *Rhizopus oryzae*. *Appl Biochem Biotechnol* 177:541–555
50. Bouras HD, Isik Z, Arikian EB, Yeddou AR, Bouras N, Chergui A, Favier L, Amrane A, Dizge N (2021) Biosorption characteristics of methylene blue dye by two fungal biomasses. *Int J Environ Stud* 78(3):365–381
51. Sintakindi A, Ankamwar B (2020) Uptake of methylene blue from aqueous solution by naturally grown *daedalea africana* and *phellinus adamantinus* fungi. *ACS Omega* 5(22):12905–12914
52. Ahmed HAB, Ebrahim SE (2020) Removal of methylene blue and Congo red dyes by pretreated fungus biomass–equilibrium and kinetic studies. *J Adv Res Fluid Mech Therm Sci* 66(2):84–100
53. Nambiar AP, Pillai R, Sanyal M, Vadikkeettil Y, Shrivastav PS (2023) A starch based sustainable bio-hybrid composite for

- surface assimilation of methylene blue: preparation, characterization, and adsorption study. *Environ Sci Adv* 2:861–876
54. Laskar N, Kumar U (2018) Adsorption of crystal violet from wastewater by modified bambusa tulda. *KSCE J Civ Eng* 22:2755–2763
55. Praveen S, Gokulan R, Pushpa TB, Jegan J (2021) Techno-economic feasibility of biochar as biosorbent for basic dye sequestration. *J Indian Chem Soc* 98(8):100107
56. Singh K, Chandra B, Gautam M (2016) Development of inexpensive adsorbent from agro-waste for phenol adsorption. *J Sci Ind Res* 75:444–451

Publisher's Note Springer Nature remains neutral with regard to jurisdictional claims in published maps and institutional affiliations.